Application of Maximum Entropy reconstruction to PISEMA spectra

D.H. Jones, S.J. Opella *

Department of Chemistry and Biochemistry, University of California, San Diego, 9500 Gilman Drive, 0307 La Jolla, CA 92093-0307, USA

Abstract

Maximum Entropy reconstruction is applied to two-dimensional PISEMA spectra of stationary samples of peptide crystals and proteins in magnetically aligned virus particles and membrane bilayers. Improvements in signal-to-noise ratios were observed with minimal distortion of the spectra when Maximum Entropy reconstruction was applied to non-linearly sampled data in the indirect dimension. Maximum Entropy reconstruction was also applied in the direct dimension by selecting sub-sets of data from the free induction decays. Because the noise is uncorrelated in the spectra obtained by Maximum Entropy reconstruction of data with different non-linear sampling schedules, it is possible to improve the signal-to-noise ratios by co-addition of multiple spectra derived from one experimental data set. The combined application of Maximum Entropy to data in the indirect and direct dimensions has the potential to lead to substantial reductions in the total amount of experimental time required for acquisition of data in multidimensional NMR experiments.
© 2005 Elsevier Inc. All rights reserved.

Keywords: Single crystal; Aligned sample; Sensitivity enhancement; Data processing; Solid-state NMR

1. Introduction

The sensitivity of NMR spectroscopy and, correspondingly, the amount of time that must be devoted to signal averaging to obtain an adequate signal-to-noise ratio is strongly affected by the method used to calculate the frequency domain spectrum from the time domain data that are acquired experimentally. Traditionally, this has been accomplished by apodization and a few other straightforward mathematical manipulations (e.g., baseline correction, zero filling, etc.) of the digitized free induction decay followed by Fourier transformation [1]. There are some trade-offs between resolution and sensitivity that can be made through the application of various apodization functions to the time domain data, but overall when Fourier transformation is employed as the principal step in data processing there are relatively few opportunities for further data manipulation. As a consequence, there is currently substantial activity in the development of alternatives to Fourier transformation for processing experimental NMR data, primarily to improve the sensitivity of the experiment [2]. The most popular alternatives included in standard software packages are Linear Prediction (LP) and Maximum Entropy (MaxEnt) [3,4] for the analysis of multidimensional solution NMR data. In this article, we describe the application of MaxEnt reconstruction as implemented in the NMR Toolkit (www.rowland.org/rnmrtk/toolkit.html) to both the indirect and direct dimensions of two-dimensional polarization inversion spin-exchange at the magic angle (PISEMA) spectra [5] of stationary samples of peptide single crystals and magnetically aligned proteins.

Applications of MaxEnt reconstruction to multidimensional solution NMR have received the most attention largely because of the time savings associated with non-linear sampling in the indirect dimensions [6–11]. However, the potential range of applications of MaxEnt reconstruction in NMR spectroscopy is much broader, including sol-

* Corresponding author. Fax: +1 858 822 4821.
  E-mail address: sopella@ucsd.edu (S.J. Opella).

id-state NMR experiments where the generally poor signal-to-noise ratios and non-exponential free induction decays limit the applications of LP because of frequency errors and the appearance of spurious peaks [12]. In addition to the obvious benefit of decreasing the amount of time devoted to signal averaging, there are advantages associated with the collection of more t_1 points at shorter times, including probe reliability and sample stability. Both are improved by the substantial reduction in the total amount of time they are subjected to high power radiofrequency irradiations, especially in high field experiments. An application of MaxEnt reconstruction to magic angle sample spinning solid-state NMR of powder samples has been described [13].

Solid-state NMR of aligned samples relies on the measurement of orientationally dependent frequencies for individual resonances as input for calculating the structures of proteins that are immobilized as part of supramolecular complexes, such as membrane bilayers [14] or virus particles [15]. A relevant feature of this NMR application is that moderate distortions of line shapes and relative intensities are readily tolerated, since only the frequencies of the resonances are of interest. This allows for more flexibility in data manipulation compared to the situation frequently encountered in multidimensional solution NMR experiments on proteins where the observation of weak peaks in the presence of strong peaks and the quantization of their intensities are often crucial. Moreover, through application of MaxEnt to both the indirect and direct dimensions, it is possible to significantly improve signal-to-noise ratios with less distortion of intensities than is generally the case when it is applied only in the indirect dimension.

2. Results

2.1. MaxEnt and non-linear sampling in t_1

PISEMA spectra are separated local field spectra [16] with high resolution in both the indirect heteronuclear dipolar coupling and the direct chemical shift frequency dimensions. The resonance frequencies in both of these dimensions are orientationally dependent because the anisotropic nuclear spin interactions are not averaged by molecular motions in stationary, aligned samples. Chemically identical sites can have different frequencies in both dimensions when the chemical shift and heteronuclear dipolar coupling interaction tensors have different orientations with respect to the direction of the applied magnetic field. The most common application is to ^{15}N-labeled amide sites in polypeptides where the ^{1}H–^{15}N heteronuclear dipolar coupling and ^{15}N chemical shift frequencies provide orientation constraints as input for calculation of the three-dimensional structure of the protein backbone [17].

Fig. 1 compares three PISEMA spectra of a ^{15}N-labeled single crystal of the model peptide N-acetyl-leucine. The spectra were obtained under identical conditions, except for the number and spacing of the t_1 increments acquired in the indirect (^{1}H–^{15}N dipolar coupling) dimension. The four unique molecular orientations of N-acetyl-leucine in the unit cell result in four resolved resonances that have the same ^{15}N chemical shift and ^{1}H–^{15}N heteronuclear dipolar coupling frequencies in all three spectra. One-dimensional spectral slices extracted from the two-dimensional spectra in the ^{1}H–^{15}N heteronuclear dipolar coupling and ^{15}N chemical shift frequency dimensions for the same resonance, indicated by the arrows, are aligned
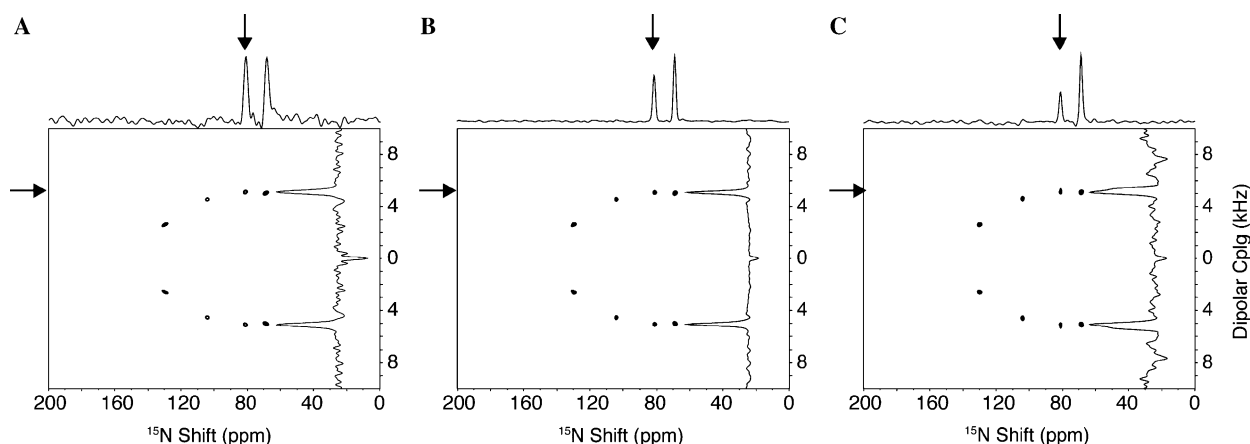

Fig. 1. Two-dimensional PISEMA spectra of a single crystal of ^{15}N-acetyl-leucine at an arbitrary orientation obtained at 700 MHz. (A) Spectrum obtained by Fourier transformation of 128 linearly sampled t_1 points that were acquired in 22 min. (B) Spectrum obtained by MaxEnt reconstruction of 32 non-linearly sampled t_1 points that were acquired in 6 min. (C) Spectrum obtained by MaxEnt reconstruction of 24 non-linearly sampled t_1 points that were acquired in 4 min. No apodization was applied to the data in the indirect (t_1) dimension. All of the data in the direct (t_2) dimension were multiplied by an exponential function corresponding to 100 Hz of line broadening followed by Fourier transformation. Two scans were acquired for each t_1 increment. The experimental acquisition parameters were 58.1 kHz ^{1}H B_1 field, 1 ms cross-polarization mix time, 5 ms acquisition time, and 5 s recycle delay. The MaxEnt reconstructions of the non-linearly sampled data sets in (B) and (C) were performed using identical values of Def and Lambda in the NMR Toolkit. The non-linear sampling schedules were calculated assuming Lorentzian line widths of 100 Hz. The signal-to-noise ratios are: (A) 32:1, (B) 175:1, and (C) 58:1.

on their respective axes in all three spectra. The spectrum in Fig. 1A was obtained in the conventional way: 128 t_1 points were sampled at equal time increments, and processed by Fourier transformation; with the free induction decays from two scans co-added for each t_1 increment, data acquisition required 22 min, and yielded a signal-to-noise ratio of 32:1 for the two-dimensional spectrum. The spectrum in Fig. 1B was obtained under identical conditions, except that only 32 non-linearly sampled t_1 points were acquired and processed using MaxEnt reconstruction. In spite of the experimental data being acquired in one-fourth the amount of time, the signal-to-noise ratio of 175:1 for the two-dimensional spectrum is substantially higher than that for the spectrum in Fig. 1A. Comparisons of the one- and two-dimensional spectra in Figs. 1A and B demonstrate that the combination of non-linear sampling and MaxEnt reconstruction in the indirect dimension is potentially capable of reducing the total time for acquisition of two-dimensional solid-state NMR spectra with little or no broadening of the resonances.

The result in Fig. 1B begs the question of how much sensitivity can be gained through the combination of non-linear sampling and MaxEnt reconstruction in the indirect dimension. In our experience with PISEMA on model peptide crystals and magnetically aligned proteins, we have found that when the non-linear sampling schedule used in the indirect dimension contains less than about one-fourth the number of points that would be acquired in the equivalent linearly sampled experiment, the resulting spectra become very sensitive to the details of the sampling schedule and are generally degraded. This is illustrated by the spectrum in Fig. 1C, which resulted from non-linear sampling of 24 points in t_1. The overall signal-to-noise ratio (58:1) is only about one-third of that in Fig. 1B (obtained from 32 t_1 points), and the spectral slices display marked

distortion in the dipolar coupling dimension as well as larger variations in the relative signal amplitudes.

Non-linear sampling and MaxEnt reconstruction of PISEMA spectra can also be applied to proteins that are immobilized and aligned as part of biological supramolecular complexes. This is illustrated in Fig. 2 with a comparison of two-dimensional PISEMA spectra of uniformly ^{15}N-labeled Pf1 bacteriophage, a nucleoprotein filament that aligns with its long axis parallel to the direction of the magnetic field. With a total mass greater that 10^7 Da, the 46-residue coat protein subunits are immobile on NMR timescales. We have previously determined the three-dimensional structure of the Pf1 coat protein using the frequencies measured in PISEMA spectra like those in Fig. 2 as input for structure calculations [15]. The PISEMA spectra are dominated by "wheel-like" patterns of resonances between about 160 and 230 ppm that are characteristic of α-helices aligned nearly parallel to the direction of the magnetic field [18,19]. Both of the spectra in Fig. 2 resulted from signal averaging of 16 scans for each t_1 point and Fourier transformation of the directly acquired data in t_2. The two-dimensional spectrum in Fig. 2A was obtained in 136 min with linear sampling of 64 t_1 points and Fourier transformation, and that in Fig. 2B in 52 min with non-linear sampling of 25 t_1 points and MaxEnt reconstruction. The spectrum in Fig. 2B was acquired in less than half the amount of time, yet its signal-to-noise ratio of 86:1 is significantly higher than the 24:1 observed in the spectrum in Fig. 2A. Notably, both spectra have similar appearances, even though many resonances are partially or completely overlapped. As seen with the data in Fig. 1, the improvement in efficiency arises from two effects of MaxEnt reconstruction of the data in the indirect dimension. The smaller number of increments acquired with non-linear sampling decreases the total
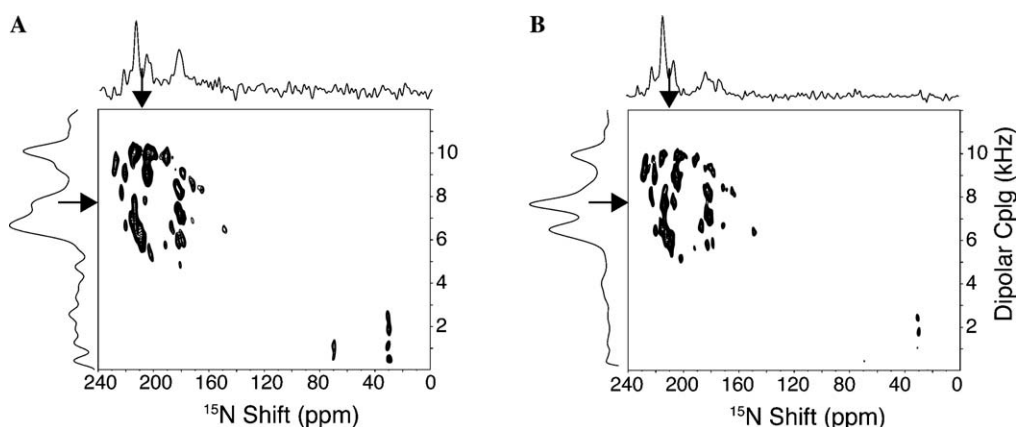

Fig. 2. Two-dimensional PISEMA spectra of uniformly ^{15}N-labeled magnetically aligned Pf1 bacteriophage obtained at 750 MHz. (A) Spectrum obtained by Fourier transformation of 64 linearly sampled t_1 points that were acquired in 136 min; the signal-to-noise ratio is 24:1. (B) Spectrum obtained by MaxEnt reconstruction of 25 non-linearly sampled t_1 points that were acquired in 52 min; the signal-to-noise ratio is 86:1. No apodization was applied to the data in the indirect (t_1) dimension. All of the data in the direct (t_2) dimension were multiplied by a Gaussian function corresponding to 100 Hz of line broadening followed by Fourier transformation. Sixteen scans were acquired for each t_1 increment. The experimental acquisition parameters were 56.8 kHz [1]H B_1 field, 1 ms cross-polarization mix time, 5 ms acquisition time, and 8 s recycle delay.

amount of experimental time; with judicious choices of the processing parameters Def and Lambda the spectra are not significantly distorted and the signal-to-noise ratios calculated using standard NMR processing software are increased. In our experience, the choice of Def should be similar to the noise level, and both the values and their ratios need to be varied while monitoring the quality of the resulting spectra to avoid those combinations of Def and Lambda that result in added noise or folded peaks [2].

2.2. MaxEnt and non-linear "sampling" in the direct dimension (t_2)

It is also possible to improve the signal-to-noise ratios of one-dimensional NMR spectra and to obtain additional gains in multidimensional spectra by applying non-linear sampling and MaxEnt reconstruction to the data acquired in the direct dimension. This relies on the differential effects of MaxEnt reconstructions on the signals and the noise when applied to different non-linear sampling schedules. Obviously, the time devoted to signal averaging is not going to be reduced by the non-linear sampling of experimental data points in the direct dimension, and this is not done. Instead, sub-sets of data points are selected from a linearly sampled experimental data set, and these artificially non-linearly sampled time domain data sets are then separately subjected to MaxEnt reconstruction to generate multiple frequency domain spectra.

The results shown in Figs. 1 and 2 demonstrate that it is feasible to select processing parameters for MaxEnt reconstruction of non-linearly sampled data, regardless of the number of data points (provided that it is not too small of a number), that yield spectra with signal-to-noise ratios higher than those resulting from Fourier transformation. These results also demonstrate that the reconstruction of non-linearly sampled data yield signals with properties, i.e., frequencies, intensities, phases, line widths, etc., that are very similar to those resulting from Fourier transformation of linearly sampled data sets. Significantly, the properties of the noise can be quite different in spectra reconstructed from different sub-sets of data extracted from the same original complete data set, and it is this feature that provides additional opportunities for data manipulation and improving the signal-to-noise ratio.

The signals resulting from MaxEnt reconstruction of differently sampled data sets have the same properties and, therefore, are coherent; however, the noise can have different properties, and is incoherent for many but not all combinations of numbers of points and non-linear sampling schedules of the time domain signals. The co-addition of frequency domain spectra where the signals are coherent and noise incoherent provided the basis for the earliest form of signal averaging in continuous wave NMR spectroscopy using the computer of average transients (CAT) [20,21]. The same principle can be extended to the co-addition of spectra obtained by MaxEnt reconstruction of different non-linearly sampled data sets. By generating multiple non-linearly sampled time domain data sets from a single linearly sampled experimental free induction decay, it is possible to perform virtual signal averaging through computation without adding to the total amount of time devoted to signal averaging.

The procedure for virtual signal averaging consists of acquiring one linearly sampled free induction decay, which would yield a spectrum by either Fourier transformation or MaxEnt reconstruction with an inadequate signal-to-noise ratio. Non-linearly sampled sub-sets of data are extracted from the complete data set corresponding to the free induction decay, the data sets are individually subjected to Max-Ent reconstruction, the noise is examined to ensure that it is uncorrelated with that of the other spectra already selected, and then the spectra are added. The process is repeated until the signal-to-noise ratio is adequate for measurement of the spectral parameters of interest.

The application of MaxEnt reconstruction to one-dimensional spectra illustrated in Fig. 3 explicates the principles of virtual signal averaging. All of the results are derived from the experimental free induction decay in Fig. 3A, which was acquired by cross-polarization [22] on the same single crystal sample of *N*-acetyl-leucine used to obtain the results shown in Fig. 1. When processed by Fourier transformation, the one-dimensional spectrum in Fig. 3B results. There are only three signals because two of the resonances have the same ^{15}N chemical shift frequency at this orientation of the crystal in the magnet. Equivalent 100 ppm segments of noise are expanded above and offset to the right of the spectra.

The dots in Fig. 3C represent the 465 digitized data points in the experimental free induction decay (Fig. 3A). When all of these data are subjected to Fourier transformation, the spectrum in Fig. 3B results; when the same data are subjected to MaxEnt reconstruction, the spectrum in Fig. 3D results. All of the spectral properties of both the signals and the noise in the spectra derived from the complete (465 points) linearly sampled time domain data by Fourier transformation (Fig. 3B) and by MaxEnt reconstruction (Fig. 3D) are essentially identical. For this example, the processing parameters were chosen so that the pairs of spectra in Fig. 3 (B (19:1) and D (19:1), and F (30:1), and H (33:1)) have similar signal-to-noise ratios. The difference spectrum in Fig. 3J, obtained by subtracting the spectrum in Fig. 3D from that in Fig. 3B, is plotted on the same vertical scale, and demonstrates that there are only very small differences between the spectra. Close inspection of the amplitudes and phases of the expanded regions of noise in Figs. 3B and D reveal minimal differences; significantly, the signal peaks are very similar in these two spectra, and subtract nearly completely. These comparisons demonstrate that spectra obtained by either Fourier transformation or MaxEnt reconstruction of the same linearly sampled time domain data set are essentially identical in all regards. In contrast, the spectra in Figs. 3F and H, which resulted from MaxEnt reconstruction of different sub-sets of the same time domain data, are similar but
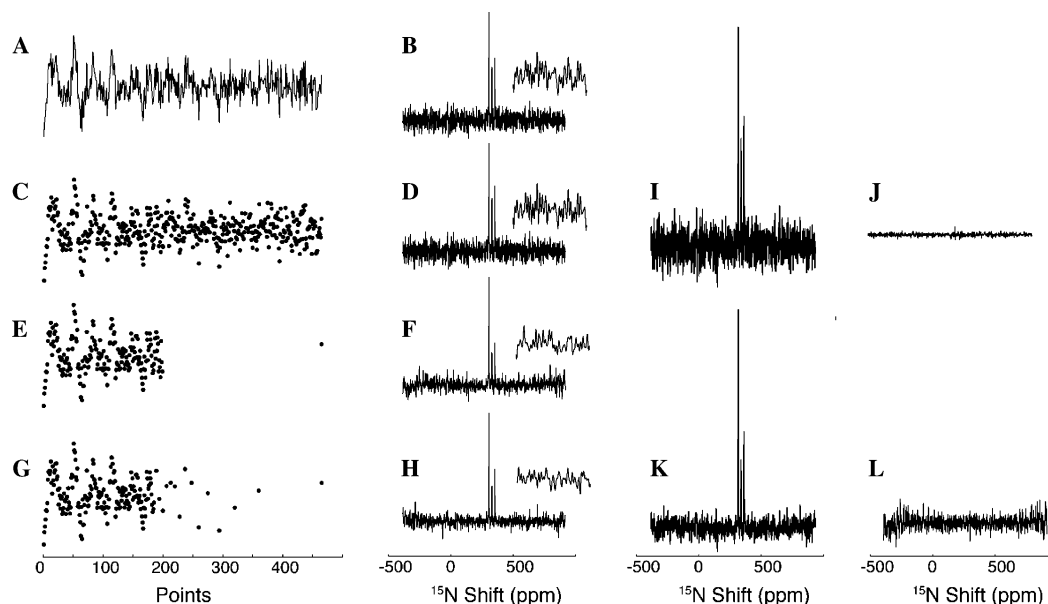
Fig. 3. Data processing in the direct dimension. (A) Experimental ^{1}H decoupled ^{15}N free induction decay obtained by cross-polarization from a single crystal of ^{15}N-acetyl-leucine obtained at 750 MHz. The experimental acquisition parameters were four scans, 62.5 kHz ^{1}H B_1 field, 1 ms cross-polarization mix time, and 6 s recycle delay. The sweep width was 100 kHz. Five hundred and twelve complex data points were collected, but only 465 are available for processing and are shown in (A) because of the effects of the digital filters. (B) Spectrum obtained by Fourier transformation of the data in (A). (C) Representation of the free induction decay in (A) using dots for the digitized data points. (D) Spectrum obtained by MaxEnt reconstruction of the data in (A). (E) Dots representing 200 non-linearly sampled data points taken from (C). (F) Spectrum obtained by MaxEnt reconstruction of the data in (E). (G) Same as (E) only with a different sampling schedule. (H) Spectrum obtained by MaxEnt reconstruction of the data in (G). An expanded 100 ppm noise region is offset above and to the right of each of the spectra in (B), (D), (F), and (H). (I) The "sum" spectrum obtained by adding spectra (B) and (D). (K) The "sum" spectrum obtained by adding spectra (F) and (H). (J) The "difference" spectrum obtained by subtracting (D) from (B). (L) The "difference" spectrum obtained by subtracting (H) from (F). The signal-to-noise ratios for the strongest peaks are: (B) 19:1, (D) 19:1, (I) 19:1, (F) 30:1, (H) 33:1, and (K) 39:1.

not identical; in particular, the signals are the same but the noise is different in the two spectra.

The dots displayed in Figs. 3E and G represent two different sub-sets of the data in Fig. 3C. They were obtained by selecting 200 points out of the full 465 point data set shown in Fig. 3C. The points near the beginning of the free induction decay are sampled more densely than those acquired at later times, reflecting the quasi-exponential weighting of the otherwise random sampling schedules selected using the "sampsched" function in the NMR Toolkit for the experimental sweep width. The signals in Figs. 3F and H, which result from MaxEnt reconstruction of the data in Figs. 3E and G, respectively, have very similar amplitudes, phases, and frequencies. The noise is quite different in these two spectra, as can be seen by close inspection of the expanded noise regions and the difference spectrum in Fig. 3L obtained by subtracting the spectrum in Fig. 3H from that in Fig. 3F. Note that neither of the two different spectra in (Figs. 3J and L) has significant signal intensity, but that the one in Fig. 3L has much larger noise intensity than the one in Fig. 3J. This demonstrates that the signals are highly correlated in both pairs of spectra; the noise is correlated when the full data set is processed, by either Fourier transformation or MaxEnt reconstruction; and the noise is uncorrelated when different non-linearly sampled data sub-sets are processed, which

can only be done with MaxEnt reconstruction because of the non-linear distribution of data points.

The correlation of noise between pairs of spectra is shown graphically in Fig. 4. The data from two pairs of expanded noise regions in Fig. 3 are plotted. The noise in the spectra in Figs. 3B and D has a very high correlation coefficient of 0.98 as shown by the correlation plot in Fig. 4A. This is consistent with the small amplitudes observed in the difference spectrum in Fig. 3J. In contrast, the noise in the spectra in Figs. 3F and H has a very low correlation coefficient of 0.00005, and this is apparent in both the correlation plot in Fig. 4B and the difference spectrum in Fig. 3L.

The differences in the pair wise correlations of the noise are also evident in the comparisons of the "sum" spectra in Figs. 3I and K obtained by adding the spectra in Figs. 3B and D and those in Figs. 3F and H, respectively. Both signals and noise in the spectrum in Fig. 3I have twice the intensity as those in either Figs. 3B or D, as expected from the addition of two highly correlated spectra. The signals in the spectrum (Fig. 3K) obtained by addition of the spectra in Figs. 3F and H are also twice as intense as those in either of the two contributing spectra, however, the noise peaks are only somewhat more intense than those in either of the contributing spectra. The comparison between the two "sum" spectra (Figs. 3I and K) is highly pertinent; it
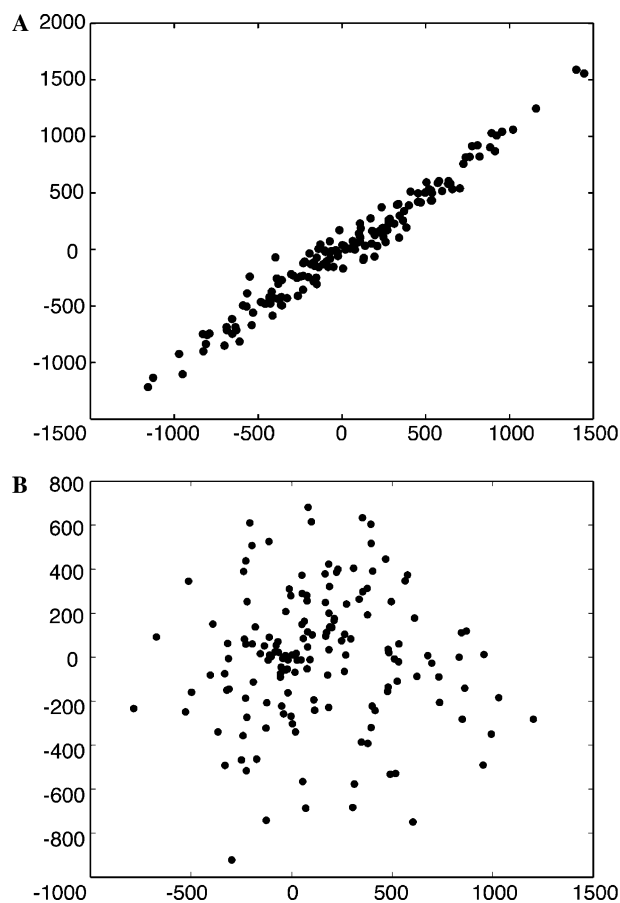
Fig. 4. Correlation plots of the expanded noise regions from the spectra in Fig. 3. The intensity of each data point is plotted versus that of the same point in the spectra that are being compared. The points are selected in order from left to right in the expanded noise regions. (A) Correlation plot for the spectra in Fig. 3B (y axis) and 3D (x axis). The correlation coefficient of 0.98 indicates that the noise is very highly correlated in these two spectra. (B) Correlation plot for the spectra in Fig. 3F (y axis) and 3H (x axis). The correlation coefficient of 0.00005 indicates that the noise is uncorrelated in these two spectra.

demonstrates that the correlated noise peaks add the same way signals do, and as a result the signal-to-noise ratios of the spectra in Figs. 3B, D, and I are identical (19:1). In contrast, the addition of spectra with uncorrelated noise gives a somewhat reduced noise level compared to the signals, resulting in a net improvement in the signal-to-noise ratio in the spectrum in Fig. 3K (39:1) compared to that in Figs. 3F (30:1) or 3H (33:1). This demonstrates that when multiple spectra with correlated signals and uncorrelated noise generated from the same time domain data are added; the signal-to-noise ratio is improved, as in conventional signal averaging.

The application of MaxEnt reconstruction methods to both dimensions of experimental PISEMA data with attendant improvements in the signal-to-noise ratio is illustrated in Fig. 5 using data obtained from a single crystal of N-acetyl leucine at a different orientation than that used for the data in Figs. 1 or 3. The two-dimensional spectrum in Fig. 5A resulted from conventional Fourier transformation

of linearly sampled data in both dimensions. Spectral slices through the largest and smallest peaks in the chemical shift frequency dimension are shown, along with expansions of noise regions. The spectrum in Fig. 5B resulted from the application of MaxEnt reconstruction to a non-linearly sampled data set in the indirect dimension and Fourier transformation of the free induction decay in the direct dimension. The spectrum in Fig. 5C resulted from a combination of MaxEnt reconstruction of non-linearly sampled points in t_1 and virtual signal averaging in the direct dimension. No apodization was applied to the data in either the indirect or direct dimensions. The gains in signal-to-noise ratios of the peaks are apparent in the spectral slices. There are little or no changes in line widths or frequencies of the resonances. There are some changes in relative intensities, however, even the weakest peaks have better signal-to-noise ratios than with conventional Fourier transformation in both dimensions (Fig. 5A) or a combination of MaxEnt in the indirect dimension and Fourier transformation in the direct dimension (Fig. 5B). We find that the suppression of weak peaks is less severe with when MaxEnt reconstruction is used in both dimensions than it is with MaxEnt reconstruction in t_1 and Fourier transformation in t_2. As a result, this approach to data processing may prove useful in applications where weak peaks need to be detected in the presence of strong peaks, in addition to its role in improving signal-to-noise ratios.

The application of MaxEnt reconstruction in t_1 and virtual signal averaging in t_2 to PISEMA data of a protein is illustrated in Fig. 6. The sample is the trans-membrane domain of Vpu labeled with ^{15}N in 20 of the 36 residues. The protein is magnetically aligned in "unflipped" bicelles. The spectrum in Fig. 6A, obtained by Fourier transformation in both dimensions has an overall signal-to-noise ratio of 177:1. By contrast, the spectrum in Fig. 6B obtained by MaxEnt reconstruction in t_1 and virtual signal averaging in t_2 has an overall signal-to-noise ratio of 6206:1. These improvements in signal to noise are mirrored in the one-dimensional spectral slices extracted at the dipolar coupling frequency marked with the arrows. Also, the MaxEnt reconstruction in the indirect dimension eliminates the truncation artifacts (sinc distortions in the baseline) associated with the intense narrow side chain resonance near 75 ppm, as previously noted by Hoch and Stern [2]. Although there are differences in the relative intensities of overlapping resonances, the resolution and overall appearance are similar in the spectra generated from the same experimental data by conventional Fourier transformation in both dimensions (Fig. 6A) and by the application of MaxEnt in both dimensions (Fig. 6B).

3. Discussion

The application of MaxEnt reconstruction to PISEMA spectra provides substantial improvements in the sensitivity of the experiment. The examples in this article are limited to two-dimensional PISEMA spectra of a single crystal of
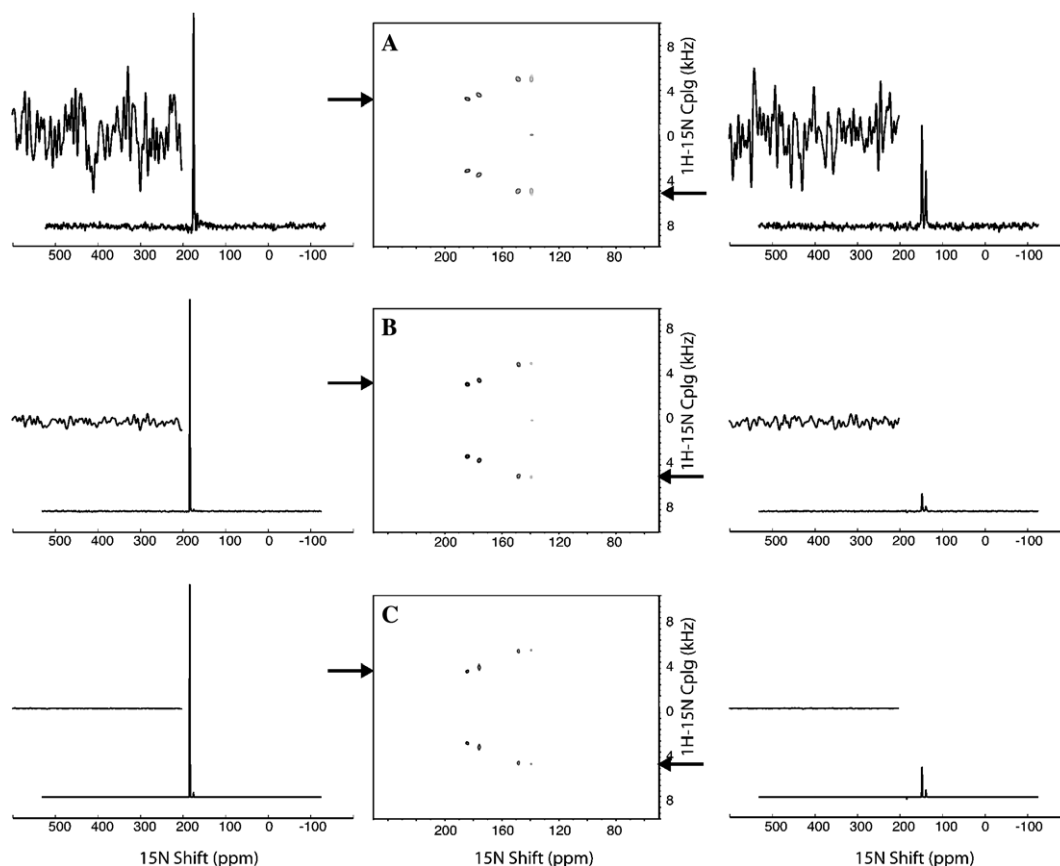
Fig. 5. Two-dimensional PISEMA spectra of a single crystal of ^{15}N-acetyl-leucine obtained at 750 MHz. (A) Spectrum obtained by Fourier transformation of 128 linearly sampled t_1 points that were acquired in 43 min. (B) Spectrum obtained by MaxEnt reconstruction of 48 non-linearly sampled t_1 points acquired in 16 min. (C) Spectrum obtained by MaxEnt reconstruction of the same data as in (B) and the application of virtual signal averaging to the data in the direct dimension. No apodization was applied to the data in the indirect (t_1) dimension. The direct (t_1) dimension data in (A) and (B) were multiplied by a Gaussian function corresponding to 100 Hz of line broadening followed by Fourier transformation. No apodization was applied to the direct (t_2) dimension data in (C). Four scans were acquired for each t_1 increment. The experimental acquisition parameters were 45.45 kHz ^{1}H B_1 field, 1 ms cross-polarization mix time, 5 ms acquisition time, and 5 s recycle delay. The arrows indicate slices taken through the strongest and weakest peak in the spectra. The sweep widths were 50 kHz in the direct dimension (t_2) and 27.8 kHz in the indirect dimension (t_1). The signal-to-noise ratios for the strongest and weakest peaks, respectively, are: (A) 199:1 and 47:1, (B) 870:1 and 25:1, and (C) 37000:1 and 1800:1.

a model peptide and magnetically aligned proteins in stationary samples. Similar applications of MaxEnt reconstruction can be applied to the variants of PISEMA that have been developed and applied to single crystals, aligned samples, and powders in stationary [5,23–28] and magic angle sample spinning experiments [29–31]. In all cases, non-linear sampling in indirect dimensions not only reduces the duration of the experiment, but also has the additional benefit of reducing the impact of the high power radiofrequency irradiations on the probe and sample.

MaxEnt can be applied in both the indirect and direct dimensions. By selecting non-linearly sampled data subsets from the complete linearly sampled free induction decay, it is possible to perform virtual signal averaging to further improve the signal-to-noise ratios without devoting additional time to signal averaging. It also results in less severe suppression of weak peaks in the presence of strong peaks compared to the application of MaxEnt in only the indirect dimension. The use of MaxEnt and in the indirect and direct dimensions has the potential to lead to substan-

tial reductions in the total amount of experimental time required for acquisition of data for multi-dimensional NMR experiments.

4. Experimental

4.1. Samples

The single crystal sample of N-acetyl-leucine used in these experiments has the dimensions of $3.0 \times 2.5 \times 1.0$ mm. It was placed at arbitrary orientations relative to the direction of the applied magnetic field, and maintained at room temperature. Different orientations of the crystal were used for the data in Figs. 1, 3, and 5.

The 50 mg/mL sample of ^{15}N-labeled Pf1 bacteriophage has been described previously [15]. The sample was maintained at 0 °C in a 5 mm glass tube in the solenoid coil of the probe.

Samples of ^{15}N-labeled membrane spanning domain of Vpu in bicelles have been described previously [32]. In
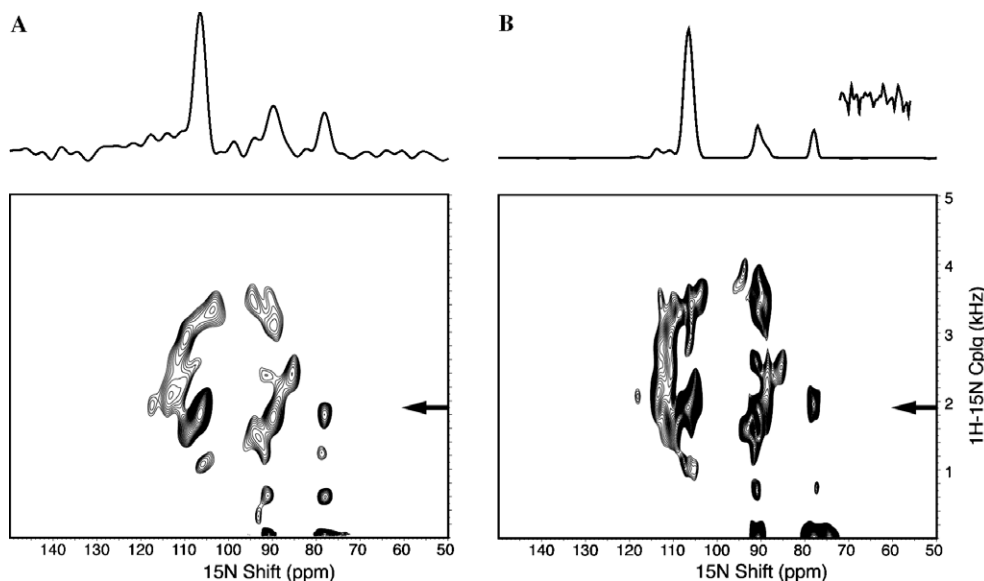
Fig. 6. Two-dimensional PISEMA spectra of the trans-membrane domain of Vpu with 20 sites labeled with ^{15}N in magnetically aligned ''unflipped'' bicelles obtained at 750 MHz. (A) Spectrum obtained by Fourier transformation of 64 linearly sampled t_1 points that were acquired in 10.25 h. The data in the direct dimension were processed with Gaussian multiplication corresponding to 100 Hz line broadening and Fourier transformation. (B) Spectrum obtained by MaxEnt reconstruction of 28 non-linearly samples t_1 points that were acquired in 4.5 h. Ninety-six scans were acquired for each t_1 increment. The processing of the data in the direct dimension is described in the Section 4. The experimental acquisition parameters were 49.0 kHz ^{1}H B_1 field, 1 ms cross-polarization mix time, 5 ms acquisition time, and 6 s recycle delay. The signal-to-noise ratios are: (A) 177:1, and (B) 6206:1. The offset noise region in (B) is expanded forty fold in the vertical dimension.

the sample used to obtain the data in Fig. 6, 20 of the 36 residues were labeled with ^{15}N.

4.2. NMR experiments

The experimental data in Fig. 1 were obtained on a spectrometer with a ^{1}H resonance frequency of 700 MHz consisting of a Bruker Avance console, a Magnex 700/62 magnet, and a home-built lumped-element probe with a 5 mm ID solenoid coil double-tuned to the ^{1}H and ^{15}N resonance frequencies. The experimental data in Figs. 2, 3, 5, and 6 were obtained on a spectrometer with a ^{1}H resonance frequency of 750 MHz consisting of a Bruker Avance console, a Magnex 750/54 magnet, and a home-built lumped-element probe with a 5 mm ID solenoid coil double-tuned to the ^{1}H and ^{15}N resonance frequencies. SPINAL-16 heteronuclear decoupling was used in all experiments during data acquisition [33,34].

4.3. Data processing

All of the spectra were processed using the NMR Toolkit (www.rowland.org/rnmrtk/toolkit.html). All of the reconstructions used exponentially weighted schedules generated using the ''sampsched'' function with 200 Hz of linewidth and the actual sweep widths as input; it was also used to select the non-linear schedules for acquisition of experimental data as well as to select the sub-sets of data extracted from complete linearly sampled data sets.

The examples of applying MaxEnt reconstruction to data in the direct dimensions in Figs. 5 and 6 used a start-

ing data set with 512 complex data points. The non-linearly sampled data sets contained 200 points. The sweep width and linewidth input into the ''sampsched'' function were varied, and 240 new data sets were generated. The correlation function was calculated for the noise in each spectrum relative to that in the starting spectrum and the intermediate summed spectra. Approximately 10% of these were found to have correlation coefficients <0.1, which were then subjected to a second filter, and that was to add each of these spectra one at a time to the previously added spectra and calculate the signal-to-noise ratio; only those that improved the signal-to-noise ratio were retained. For demonstration purposes, the 12 best data sets were added together to yield the spectrum in Fig. 5C. These same twelve schedules were then applied to the protein data shown in Fig. 6. The second level of checking of signal-to-noise ratios was carried out, and eight of the data sets were found to improve the signal-to-noise ratio and were co-added to give the results shown in the figure.

The signal-to-noise ratios of the two-dimensional spectra were calculated in Sparky (www.cgl.ucsf/home/Sparky/), and in MatLab (www.mathworks.com/products/matlab/) for one-dimensional spectra using the same definition. The signal-to-noise ratio is defined as the amplitude of the selected peak (or maximum peak) divided by the standard deviation of the noise.

References

[1] R.R. Ernst, W.A. Anderson, Application of Fourier transform spectroscopy to magnetic resonance, Rev. Sci. Instrum. 37 (1966) 93–102.

[2] J.C. Hoch, A.S. Stern, NMR Data Processing, Wiley, 1996.

[3] S. Sibisi, Two-dimensional reconstructions from one-dimensional data by maximum entropy, Nature 301 (1983) 134–136.

[4] S. Sibisi, J. Skilling, R.G. Brereton, E.D. Laue, J. Staunton, Maximum entropy signal processing in practical NMR spectroscopy, Nature 311 (1984) 446–447.

[5] C.H. Wu, A. Ramamoorthy, S.J. Opella, High resolution heteronuclear dipolar solid-state NMR spectroscopy, J. Magn. Reson. A 109 (1994) 270–272.

[6] P.J. Hore, NMR data processing using tge maximum entropy method, J. Magn. Reson. 62 (1985) 561–567.

[7] J.C.J. Barna, E.D. Laue, Conventional and exponential sampling for 2D NMR experiments with application to a 2D NMR spectrum of a protein, J. Magn. Reson. 75 (1987) 384–389.

[8] D.S. Stephenson, Linear prediction and maximum entropy methods in NMR spectroscopy, Prog. NMR Spectrosc. 20 (1988) 515–626.

[9] P. Schmieder, A.S. Stern, G. Wagner, J.C. Hoch, Improved resolution in triple resonance spectra by non-linear sampling in the constant time domain, J. Biomol. NMR 4 (1994) 483–490.

[10] D. Rovnyak, D.P. Frueh, M. Sastry, Z.Y. Sun, A.S. Stern, J.C. Hoch, G. Wagner, Accelerated acquisition of high resolution triple-resonance spectra using non-uniform sampling and maximum entropy reconstruction, J. Magn. Reson. 170 (2004) 15–21.

[11] D. Rovnyak, J.C. Hoch, A.S. Stern, G. Wagner, Resolution and sensitivity of high field nuclear magnetic resonance spectroscopy, J. Biomol. NMR 30 (2004) 1–10.

[12] A.S. Stern, K.B. Li, J.C. Hoch, Modern spectrum analysis in multidimensional NMR spectroscopy: comparison of linear-prediction extrapolation and maximum-entropy reconstruction, J. Am. Chem. Soc. 124 (2002) 1982–1993.

[13] D. Rovnyak, C. Filip, B. Itin, A.S. Stern, G. Wagner, R.G. Griffin, J.C. Hoch, Multiple-quantum magic-angle spinning spectroscopy using nonlinear sampling, J. Magn. Reson. 161 (2003) 43–55.

[14] S.J. Opella, F.M. Marassi, Structure determination of membrane proteins by NMR spectroscopy, Chem. Rev. 104 (2004) 3587–3606.

[15] D.S. Thiriot, A.A. Nevzorov, L. Zagyanskiy, C.H. Wu, S.J. Opella, Structure of the coat protein in Pf1 bacteriophage determined by solid-state NMR spectroscopy, J. Mol. Biol. 341 (2004) 869–879.

[16] R.K. Hester, J.L. Ackerman, B.L. Neff, J.S. Waugh, Separated local field spectra in NMR: determination of structure of solids, Phys. Rev. Lett. 36 (1976) 1081–1083.

[17] S.J. Opella, P.L. Stewart, K.G. Valentine, Protein structure by solid-state NMR spectroscopy, Q. Rev. Biophys. 19 (1987) 7–49.

[18] F.M. Marassi, S.J. Opella, A solid-state NMR index of helical membrane protein structure and topology, J. Magn. Reson. 144 (2000) 150–155.

[19] J. Wang, J. Denny, C. Tian, S. Kim, Y. Mo, F. Kovacs, Z. Song, K. Nishimura, Z. Gan, R. Fu, J.R. Quine, T.A. Cross, Imaging membrane protein helical wheels, J. Magn. Reson. 144 (2000) 162–167.

[20] O. Jardetzky, N.G. Wade, J.J. Fischer, Proton magnetic resonance investigation of enzyme-coenzyme complexes, Nature 9 (1963) 183–184.

[21] M.P. Klein, G.W. Barton, Enhancement of signal-to-noise ratio by continuous averaging: application to magnetic resonance, Rev. Sci. Instrum. 34 (1963) 754–759.

[22] A. Pines, M.G. Gibby, J.S. Waugh, Proton-enhanced nuclear induction spectroscopy. A method for high resolution NMR of dilute spins in solids, J. Chem. Phys. 56 (1972) 1776–1777.

[23] A.A. Nevzorov, S.J. Opella, A "Magic Sandwich" pulse sequence with reduced offset dependence for high-resolution separated local field spectroscopy, J. Magn. Reson. 164 (2005) 182–186.

[24] D.K. Lee, T. Narasimhaswamy, A. Ramamoorthy, PITANSEMA, a low-power PISEMA, solid-state NMR experiment, Chem. Phys. Lett. 399 (2004) 359–362.

[25] K. Yamamoto, D.K. Lee, A. Ramamoorthy, Broadband-PISEMA solid-state NMR spectroscopy, Chem. Phys. Lett. 407 (2005) 289–293.

[26] A. Ramamoorthy, Y. Wei, D.K. Lee, PISEMA solid-state NMR spectroscopy, Ann. Rep. NMR Spec. 52 (2004) 1–52.

[27] S.V. Dvinskikh, H. Zimmermann, A. Maliniak, D. Sandstrom, Separated local field spectroscopy of columnar and nematic liquid crystals, J. Magn. Reson. 163 (2003) 46–55.

[28] S.V. Dvinskikh, D. Sandstrom, Frequency offset refocused PISEMA-type sequences, J. Magn. Reson. 175 (2005) 163–169.

[29] A. Ramamoorthy, S.J. Opella, Two-dimensional chemical shift/heteronuclear dipolar coupling spectra obtained with polarization inversion spin exchange at the magic angle and magic-angle sample spinning (PISEMAMAS), Solid State NMR 4 (1995) 387–392.

[30] K. Yamamoto, V.L. Ermakov, D.K. Lee, A. Ramamoorthy, PITANSEMA-MAS, a solid-state NMR method to measure heteronuclear dipolar couplings under MAS, Chem. Phys. Lett. 408 (2005) 118–122.

[31] S.V. Dvinskikh, H. Zimmermann, A. Maliniak, D. Sandstrom, Heteronuclear dipolar recoupling in liquid crystals and solids by PISEMA-type pulse sequences, J. Magn. Reson. 164 (2003) 165–170.

[32] S.H. Park, A.A. Mrse, A.A. Nevzorov, M.F. Mesleh, M. Oblatt-Montal, M. Montal, S.J. Opella, Three-dimensional structure of the channel-forming trans-membrane domain of virus protein "u" (Vpu) from HIV-1, J. Mol. Biol. 333 (2003) 409–424.

[33] B.M. Fung, A.K. Khitrin, K. Ermolaev, An improved broadband decoupling sequence for liquid crystals and solids, J. Magn. Reson. 142 (2000) 97–101.

[34] N. Sinha, C.V. Grant, C.H. Wu, A.A. De Angelis, S.C. Howell, S.J. Opella, SPINAL modulated decoupling in high field double- and triple-resonance solid-state NMR experiments on stationary samples, J. Magn. Reson. 177 (2005) 180–185.